Materials Science & Engineering A 566 (2013) 134–142

Contents lists available at SciVerse ScienceDirect

Materials Science & Engineering A

journal homepage: www.elsevier.com/locate/msea

High-temperature-oxidation-induced ordered structure in Inconel 939 superalloy exposed to oxy-combustion environments

Jingxi Zhu [a,b,*], Adam Wise [b], Thomas Nuhfer [b], Gordon R. Holcomb [c], Paul D. Jablonski [c], Seetharaman Sridhar [a,b], David E. Laughlin [b]

[a] National Energy Technology Laboratory, Pittsburgh, PA 15236, USA
[b] Department of Materials Sciences and Engineering, Carnegie Mellon University, Pittsburgh, PA 15213, USA
[c] National Energy Technology Laboratory, Albany, OR 97321-2198, USA

ARTICLE INFO

Article history:
Received 15 November 2012
Accepted 27 December 2012
Available online 4 January 2013

Keywords:
Oxy-fuel combustion
High temperature oxidation
Ordered structure
Inconel 939 superalloy
High-resolution transmission electron microscopy

ABSTRACT

In the integrated oxy-fuel combustion and the turbine power generation system, turbine alloys are exposed to high temperature and an atmosphere comprised of steam, CO_2 and O_2. While surface and internal oxidation of the alloy takes place, the microstructure in the subsurface region also changes due to oxidation that results in the loss of the strengthening precipitates. In an earlier study of the oxidation of Inconel 939 Ni-based superalloy exposed to oxy-fuel combustion environment for up to 1000 h, a high-temperature-oxidation-induced phase transformation in the sub-surface region was noticed and a two-phase region formed at the expense of strengthening γ' phase. While one of the two phases was identified as the Ni-matrix γ solid solution, face-center-cubic) phase, the other product phase remained unidentified. In this study, the crystal structure of the unknown phase and its orientation relationship with the parent Ni-matrix phase was investigated through electron diffraction and high-resolution transmission electron microscopy. It was determined that the crystal structure of the unknown phase could be modeled as a ternary derivative of the ordered η-Ni_3Ti phase ($D0_{24}$) structure with lattice parameters of a=.5092 nm and c=.8336 nm, α=90°, β=90° and γ=120°.

1. Introduction

While new and promising oxy-fuel combustion turbine power generation systems are being developed, materials performance of candidate superalloys is a vital area of research. For the high-pressure turbines that experience the highest temperatures, materials with higher temperature capability than that of the conventional turbines is required [1,2]. Among the essential properties of the candidate materials, such as creep strength [3], oxidation resistance [4] becomes more and more important with increasing temperature of operation to the further development of the oxy-combustion technology [1,2].

Inconel 939 is a nickel-based superalloy that is being used in blades of gas turbines that can operate at temperatures up to 1123 K (850 °C) [5] and the structure of the alloy is characterized by the γ solid-solution matrix and the γ' precipitates that are critical for the mechanical properties. Relatively high volume fraction of γ' precipitates can be achieved through heat treatments [6]. However, sufficient knowledge is also required regarding the stability and degradation of the strengthening γ' precipitates under service environments.

In an earlier work [7], the high-temperature oxidation microstructure of the Inconel 939 superalloy was examined for exposures to a series of oxy-combustion environments for a number of exposure times ranging between 250 and 1000 h at temperatures between 903 and 1094 K. It was found that the surface and subsurface degradation resulted from high temperature oxidation due to the service environment extended deeper into the bulk alloy beyond the presence of oxides.

The general oxidation microstructure of Inconel 939 included an external scale, an internal oxidation zone and a depletion zone in which the γ' strengthening precipitates were depleted. The depletion zone was of particular interest because a large amount of twinning was observed (and hence dubbed the "twinning zone") and the alloy in this region partitioned into two phases: a Ni-matrix (face-centered-cubic structure, FCC) and an unknown phase that was abbreviated as U phase. Thermo-Calc (version S) [8] predicted the following phase transformation to be favored by thermodynamic equilibrium based on the overall chemistry of the

* Corresponding author at: Department of Materials Sciences and Engineering, Carnegie Mellon University, Pittsburgh, PA 15213, USA. Tel.: +1 412 268 5708; fax: +1 412 268 7596.
E-mail addresses: jingxiz@andrew.cmu.edu (J. Zhu), adamwise@andrew.cmu.edu (A. Wise), tn06@andrew.cmu.edu (T. Nuhfer), Gordon.Holcomb@NETL.DOE.GOV (G.R. Holcomb), Paul.Jablonski@NETL.DOE.GOV (P.D. Jablonski), sridhars@andrew.cmu.edu (S. Sridhar), dl0p@andrew.cmu.edu (D.E. Laughlin).

0921-5093/$ - see front matter © 2013 Elsevier B.V. All rights reserved.
http://dx.doi.org/10.1016/j.msea.2012.12.074

twinning zone:

$$(\gamma+\gamma')_{\text{depleted of Al}} \rightarrow FCC_{\text{solid solution}}+\eta \quad (1)$$

indicating the U phase being η phase (prototype is Ni_3Ti, $D0_{24}$). However, electron diffraction pattern showed extra superlattice reflections that were forbidden for η phase and could not be resulted from double diffraction. Preliminary results suggested that the U phase might have a FCC derivative crystal structure. This work is the continuation of the earlier effort, aiming to understand the crystal structure of the U phase through electron diffraction and high-resolution transmission electron microscopy (HR-TEM). With more results available, it became clear that the crystal structure of the U phase was not a FCC derivative; rather it was crystallographic derivative of the η phase.

2. Experimental

Bare alloy coupons of Inconel 939 were isothermally oxidized in simulated oxy-combustion atmospheres of $H_2O+CO_2+O_2$ mixed at different ratios. The nominal composition of the alloy is shown in Table 1. A range of combinations of temperatures and exposures times was tested. The details of these oxidation conditions can be found in Ref. [7]. The furnace heating and cooling rates were slow, on the order of 100–200 K per hour. The alloy coupon oxidized at 1094 K for 1000 h in the atmosphere of steam $+20\%$ $CO_2+.2\%$ O_2 was chosen as the case study for phase identification. The oxidized alloy was then mounted, and a metallographic cross section was prepared by fine polishing to 1 μm using diamond suspensions.

Transmission electron microscopy (TEM) specimens were prepared with a Nova 600 DualBeam system (FEI Company, Eindhoven, Netherlands) (electron beam/focused ion beam [FIB]) by in-situ liftout technique. The specimen was sampled at approximately half depth of the twinning zone. The specimens were fine polished to electron-transparent with 30 kV focused Ga^+ ion beam at a current of .1 nA, and finally cleaned with a 5 kV ion beam at a current of 50 pA.

An FEI Tecnai F20 transmission electron microscope (TEM) (acceleration voltage is 200 kV) was used for general imaging and obtaining electron diffraction patterns. An FEI Titan 80–300 transmission electron microscope equipped with a spherical aberration corrector and working under an acceleration voltage of 300 kV was used for high-resolution (HR) imaging and obtaining energy dispersive X-ray spectra (EDS) in scanning transmission electron microscopy (STEM) mode.

Phase contrast image simulation was carried out with the QSTEM software package developed by Koch [9]. The structures were initially constructed with the CrystalMaker software package. The outputs were then converted to the QSTEM format. Once in QSTEM, the settings for the Titan 80–300 were used in the simulation. Our values were: acceleration voltage: 300 kV, defocus: −8 nm, Cs: .011 mm, Cc: 1.2 mm, convergence angle: .15 mrad, and 1024×1024 samples across a 25 by 25 Å sample size. Slice thickness was set at 2 Å per slice. The QSTEM package has an option for simulating thermal diffuse scattering by running multiple simulations with slight variations in atomic position simulating atomic thermal vibrations, then summing the varied exit waves into a final exit wave incorporating thermal variation in the atomic positions. This option was used with 50 variations, set for a temperature of 300 K.

Table 1
The nominal composition of the Inconel 939 alloy, in weight percent.

Ni	Co	Cr	Al	Ti	Ta+Nb	W	C
48.36	18.9	22.5	1.9	3.8	2.4	2	.14

3. Results

Fig. 1 shows the crosssection of the overall oxidation structure of the study alloy, after 1000 h of isothermal oxidation under three simulated oxy-combustion conditions. The oxidation atmospheres are indicated in the micrographs. SEM micrographs of the alloy oxidized under the case study condition can be found in Ref. [7]. The oxidation structure was comprised of an external scale, an internal oxidation zone and a so-called twinning zone. Beneath the twinning zone, the base alloy remained unaffected by the high temperature oxidation and in its stabilized $\gamma+\gamma'$ microstructure.

The external scale was mainly Cr_2O_3. In the case of Inconel 939 alloy, the intergranular thread-like internal oxides were typically Al_2O_3, sometimes TiO_x, and/or $NiAl_2O_4$ under certain oxidation conditions [10]. The region beneath the internal oxidation zone was called the "twinning zone" because a large number of grains appeared to be twins of one another in this region. In fact, the twinning zone was comprised of a Ni-matrix (solid solution with face-center-cubic crystal structure) and the slab-shaped grain that appeared in a brighter contrast, i.e. the so-called "U phase". A large number of the Ni-matrix grains were twinned. The formation of the U phase was closely related to the progression of internal oxides into the base alloy. When the internal oxide-forming elements, i.e. Al and Ti, were depleted from the $\gamma+\gamma'$ microstructure of the base alloy, phase transformation occurred. The twinning zone microstructure was the result of such phase transformation.

3.1. The twinning-zone microstructure and electron diffraction analysis

An electron-transparent specimen was prepared by the in-situ lift-out technique with its plane view relative to the surface of the alloy oxidized at 1094 K for 1000 h in the atmosphere of steam $+20\%$ $CO_2+0.2\%$ O_2. A backscattered electron (BSE) image of the specimen is shown in Fig. 2a, and b is a TEM bright field micrograph of the U phase grain and its neighboring Ni-matrix. The U phase grains always appeared in a high-aspect ratio slab shape and were almost always delineated by straight boundaries. Stacking faults are also present parallel to the phase boundary between the Ni-matrix and U phase.

Selected-area zone-axis diffraction (ZAD) patterns (Fig. 2c) were obtained from the U phase grain shown in Fig. 2b. The specimen was tilted to each of the zone-axis orientations following the Kikuchi lines observed in the microscope, which are also shown in Fig. 2c. By obtaining d-spacings from these diffraction patterns and comparing them to the diffraction patterns simulated with CaRine v3.1 software package, it was found that the fundamental reflections in these patterns closely matched the simulated pattern of the hexagonal η phase (prototype is Ni_3Ti, $D0_{24}$). This phase was first reported by Laves and Wallbaum [11] in 1939. Therefore, the ZAD patterns and the Kikuchi bands shown in Fig. 2c were indexed with hexagonal indices of η phase. However, extra superlattice reflections that were forbidden for η phase were also seen in these patterns, and they could not have resulted from double diffraction. For instance, in the $[1\bar{1}.0]_\eta$ pattern,[1] the allowed superlattice reflections for η phase are at the $1/2\vec{g}_{<220>}$ locations ($\vec{g}_{hkl}$ refers to the reciprocal vectors), but extra reflections can also be seen at $1/2\vec{g}_{<004>}$ and $1/2\vec{g}_{<22\bar{4}>}$

[1] For the hexagonal crystallography system, the 3-indices notations are used for reciprocal space vectors and directions, etc.; and the 4-indices notations are used for real space zone axises and planes, etc.

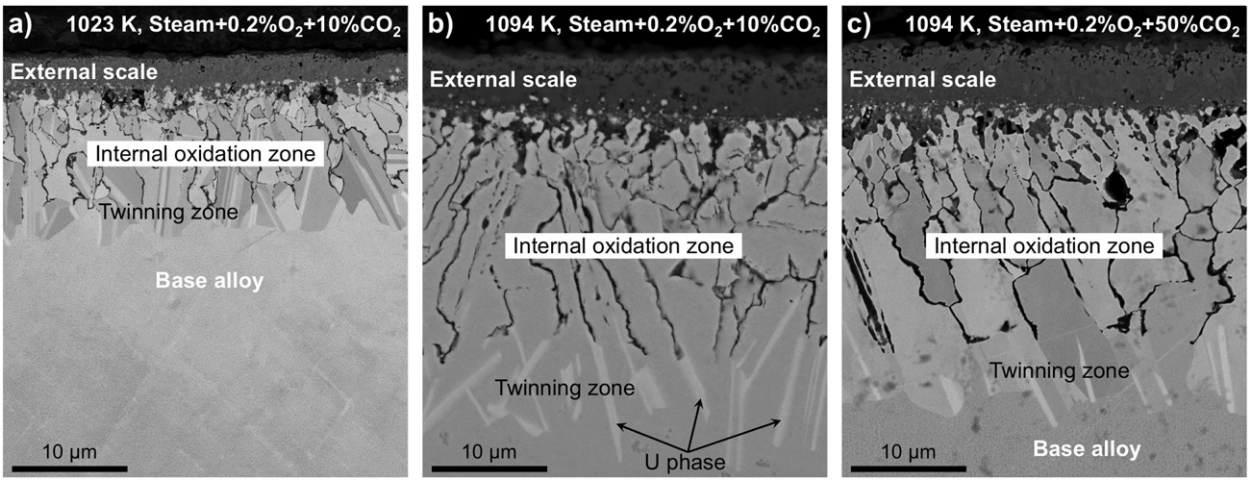

Fig. 1. Backscattered electron (BSE) image of cross-sections of Inconel 939 alloys after 1000 h of isothermal oxidation at (a) 1023 K, (b) 1094 K and (c) 1094 K in a higher CO_2 percentage atmosphere.

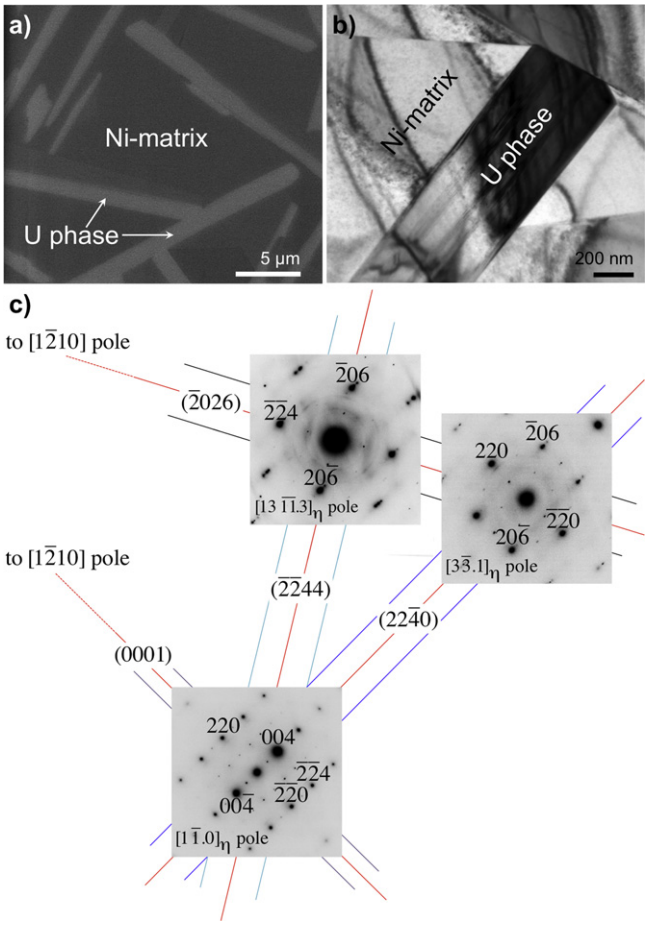

Fig. 2. (a) BSE-SEM micrograph of the thin foil lifted out from approximately half depth of the twinning zone, (b) bright field TEM image of a U phase grain, from which the ZAD patterns in (c) were obtained, with corresponding zone axes [1$\bar{1}$.0], [3$\bar{3}$.1] and [13$\bar{1}\bar{1}$.3] ([1$\bar{1}$0], [3$\bar{3}$1] and [5$\bar{3}$1] in three-index notation, respectively), along with the indexed Kikuchi bands observed in the microscope.

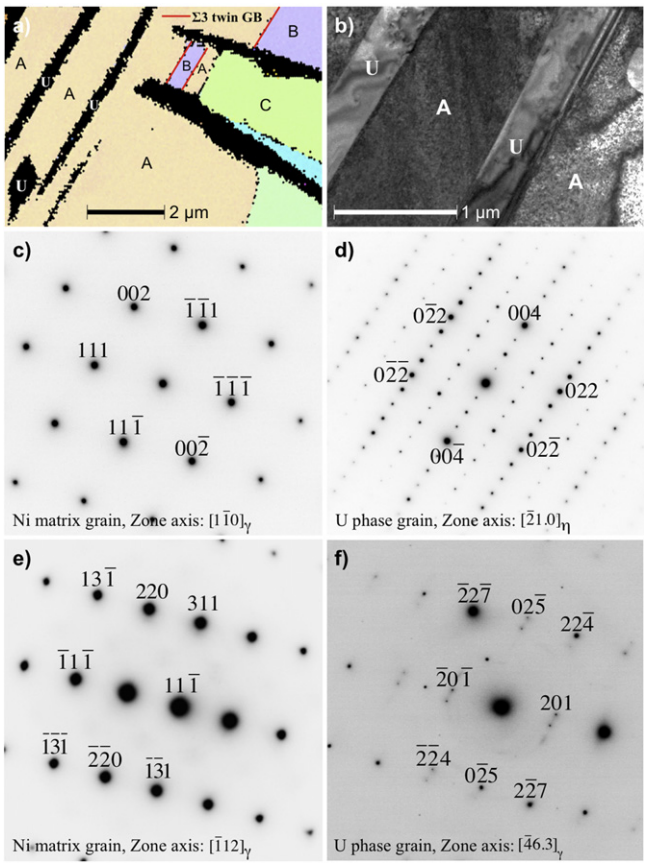

Fig. 3. (a) Inverse pole figure (IPF) orientation map of the electron transparent foil; (b) the bright field micrograph; (c) the [1$\bar{1}$0]$_\gamma$ zone axis diffraction (ZAD) pattern taken from grain A; (d) the [$\bar{2}$1.0]$_\eta$ pattern of the U phase grain at the same specimen tilts as (c); (e) the [$\bar{1}$12]$_\gamma$ diffraction pattern taken from grain A and (f) [$\bar{4}$6.3]$_\eta$ ZAD pattern of the U phase grain at the same specimen tilts as (e).

locations. This suggested that additional atomic ordering existed, which gave rise to extra superlattice reflections.

In the previous study [7], it was shown that some neighboring U phase and Ni-matrix grains were configured such that the longer direction of the U phase grain was parallel to the twin boundaries of the neighboring Ni-matrix grains. Such an example is shown in Fig. 3a. In this inverse pole figure (IPF) orientation map, the Ni-matrix grains labeled with "A" and "B" are twins. The black areas labeled by "U" are the U phase grains that are believed to have precipitated from the "A" Ni-matrix grain. The U phase slabs are parallel to the twin boundaries between A and B. In this case, we say the "U" precipitates are related to "A" grains, and the "A" grain is the parent grain of the "U" precipitates. A bright field image of the "A" and "U" grains is shown in Fig. 3b.

Because of the relation between grains "A" and "U", when the specimen was tilted to certain zone axis orientations of the "A" grain, the "U" grain was also at a zone axis orientation of its own.

Fig. 3c is the $[1\bar{1}0]_\gamma$ ZAD pattern of the "A" grain and Fig. 3d is a $[2\bar{1}0]_\eta$ ZAD pattern of the "U" grain taken at the same specimen orientation. Fig. 3e and f shows another pair of ZAD patterns in which the $[\bar{1}12]_\gamma$ zone of "A" grain is parallel to the $[\bar{4}6.3]_\eta$ zone of the U grain. The experimental $[\bar{4}6.3]_\eta$ zone pattern shown in Fig. 3f deviated slightly from the perfect zone axis orientation so that some reflections were seen to split into two spots, such as $\pm[201]^*$ (* denotes the directions in the reciprocal space). By simulating the kinematical patterns with CaRine v3.1 software, such splitting of spots can be seen with a large excitation error (Δs), i.e. $\Delta s \geq .038\ \text{Å}^{-1}$. Specimen bending could also contribute to the excitation error.

Two things can be noticed when comparing these ZAD patterns. First, the U phase and Ni-matrix can be found to have the following orientation relationship:

$$(11\bar{1})_\gamma \| (00.1)_\eta$$

$$[1\bar{1}0]_\gamma \| [2\bar{1}.0]_\eta$$

The close-packed planes, i.e. the $(11\bar{1})$ plane of the Ni-matrix and the (00.1) plane of the U phase (adopting the hexagonal indices of η phase), are coherent; the close-packed directions, i.e. the $[1\bar{1}0]$ direction in the Ni-matrix and the $[2\bar{1}.0]$ direction of the U phase, are parallel. Second, in the $[2\bar{1}.0]_\eta$ SAD pattern (Fig. 3d), besides the reflections allowed by the η phase, extra superlattice reflections were also visible in the $[004]^*_\eta$ direction at $n/4\vec{g}_{<004>}$ ($n=1, 2, 3$).

The lattice parameters were obtained from these diffraction patterns. For the U phase, $a=.5092$ nm and $c=.8336$ nm adopting a hexagonal unit cell of the η phase; and for Ni-matrix (γ solid solution) $a=.3610$ nm. These diffraction patterns will be further analyzed along with high-resolution TEM imaging in the discussion section.

3.2. High-resolution TEM imaging of the U precipitates

To further examine the atomic positions in the U phase, high-resolution TEM images were taken from U phase grains. A region containing a phase boundary between the Ni-matrix and the U phase is displayed in Fig. 4. Both the Ni-matrix grain and the U phase grain were simultaneously in zone-axis orientations, as indicated by the diffraction patterns. The Ni-matrix was at $[1\bar{1}0]_\gamma$ zone axis orientation while the U phase was at $[2\bar{1}.0]_\eta$. In the enlarged portion on the U phase side, repeating planes that appeared brighter can be cleared identified. When measuring the planar spacing between them, and comparing it to that of the {111} planes of the Ni-matrix, the former was 4 times of the latter. This is in accordance with the earlier d-spacing measurement from the ZAD diffraction patterns.

From the atomic-resolution lattice image obtained from the U phase grain shown in Fig. 5a, at the zone axis of $[2\bar{1}.0]_\eta$, the stacking sequence along the [00.1] direction was identified to be ABaCA, as displayed in the micrograph in Fig. 5b. The atoms in "A" and "a" planes were at the same stacking position but might have different chemistries, due to the difference observed in intensity profile in Fig. 5b along the sampling line in the [00.1] direction. This is different from the η-Ni_3Ti structure whose stacking sequence along the [00.1] direction is ABACA, i.e. all the planes have the same composition.

3.3. Analytical microscopy results

A 500-nm long elemental profile across the phase boundary between Ni-matrix and U phase was obtained with STEM-EDS. The beam spot size used for acquiring spectra was approximately 1 nm, and the profile was collected along the line with intervals of 5 nm. The micrograph and the profile are shown in Fig. 6. The quantification results showed similar elemental partition as shown in the previous study [7] using SEM–EDS mapping, i.e. elements including Ni, Ta, Ti, Nb and Al enriched in the U phase while Co and Cr were ejected into Ni-matrix. The concentration profiles of the abovementioned elements also displayed continuity across the phase boundary. As expected, the diffusivities of the elements in the U phase (ordered) were smaller as can be seen by comparing the concentration gradient on the two sides of the phase boundary (Table 1).

4. Disscusion

4.1. The crystal structure of the U phase

By examining the electron diffraction patterns, it was found that the fundamental reflections of the U phase closely matched those of the η-Ni_3Ti ($D0_{24}$) phase, whose structural data [12] and unit cell are shown in Table 2 and Fig. 7, respectively. The stacking sequence of this hexagonal close-packed structure is ABACA as indicated in the figure. The presence of extra superlattice reflections from U phase suggested that additional ordering is present for the U phase crystal structure. Thus, to resolve the crystal structure of the U phase, we based the structure on that of the η-Ni_3Ti ($D0_{24}$), and introduced additional atoms so that the

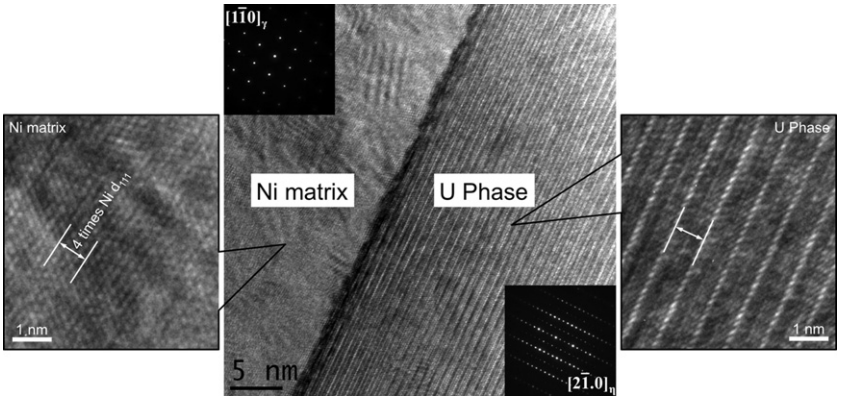

Fig. 4. High-resolution bright field image of a phase boundary between the Ni-matrix and the U phase, which are simultaneously in zone axis specimen orientation, as shown by the ZAD patterns.

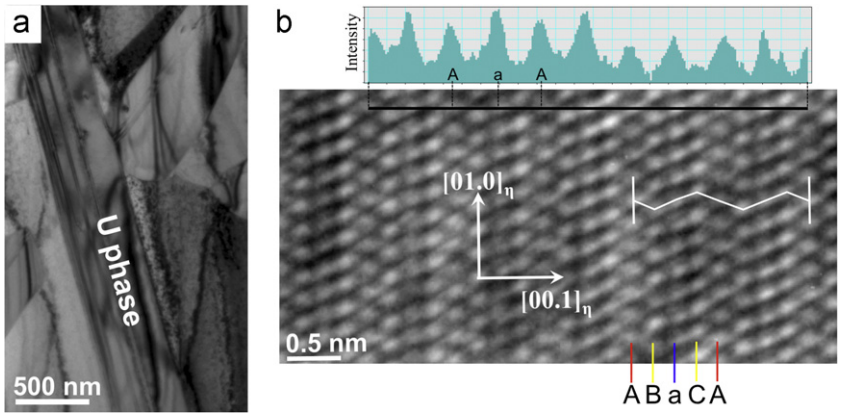

Fig. 5. (a) Bright field micrograph of the U phase grain where the HR-TEM images were taken and (b) HR-TEM image that shows the stacking sequence of the U phase.

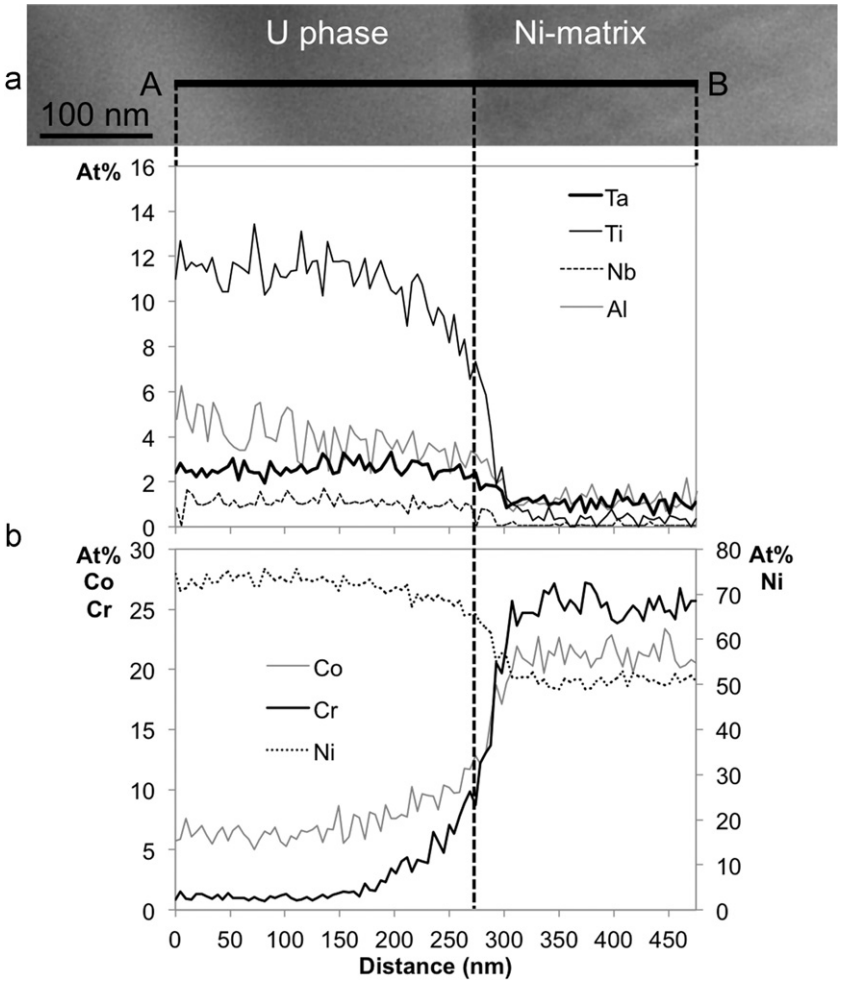

Fig. 6. (a) The high-angle-annular-dark-filed STEM micrograph of the U phase/Ni-matrix phase boundary. An elemental line profile was acquired along line AB using EDS with a step size of 5 nm. (b) The corresponding quantified elemental line profile. The elements that were included in the quantification were: Ni, Ti, Ta, Co, Cr, Nb and Al.

modified structure could give rise to matching diffraction patterns to the ones obtained experimentally.

Fig. 8 compares the simulated diffraction patterns of the η-Ni_3Ti phase to the experimental diffraction patterns obtained from the U phase at zone axes orientations of $[1\bar{1}.0]$ and $[1\bar{2}.0]$. At both zone axis orientations, η phase shows systematic absence of reflections $\{00l\}$, when $l=2n+1$, because of the presence of a 6_3 screw axis and a c glide plane in its space group; the reflections $\{0,0,2n\}$, when n is odd, are missing because of the double hexagonal stacking. In the two experimental patterns from the U phase, the intensities are clearly seen at $\{002\}$ positions. $\{001\}$ and $\{003\}$ reflections were also visible in the $[1\bar{1}.0]$ pattern of the U phase.

From the STEM–EDS analysis shown in Fig. 6, the bulk composition of the major elements in the U phase was obtained by averaging over the first 150 nm of the line profile inside the U phase grain, avoiding the concentration gradient near the phase boundary. The resulting composition is displayed in Table 3 in atomic percentages. It was evident that heavy elements such as Ta and Nb were enriched in the U phase up to 3.23 at% and

1.65 at%, respectively. It is known that all Ti sites can be randomly substituted by Al atoms in ordered Ni–Ti intermetallic phases [13], thus, for simplicity, Al and Ti will be treated as Ti. On the other hand, Nb was found to preferentially occupy particular Ti site [14], such that the system became ternary instead of binary. Also, Nb and Ta belong to the same column in the periodic table. To enhance the contrast in high-resolution TEM simulation, Nb and Ta will be treated as Ta due to a bigger atomic number difference between Ta and Ni. Therefore, the alloy system is simplified into a ternary system of Ni-Ti-Ta.

Table 2
The structure of η-Ni_3Ti phase [12].

Standard formula:	$TiNi_3$					
System	Hexagonal					
Space group	$P6_3/mmc$ (no. 194)					
Cell parameters	a=.510, b=.510, c=.830 nm, α=90°, β=90° and γ=120°					
Site	Elements	Wyckoff no.	Site symmetry	x	y	z
Ni1	Ni	6*h*	mm2	1/6	1/3	1/4
Ni2	Ni	6*g*	.2/m	1/2	0	0
Ti1	Ti	2*d*	$\bar{6}$m2	1/3	2/3	3/4
Ti2	Ti	2*a*	$\bar{3}$m.	0	0	0

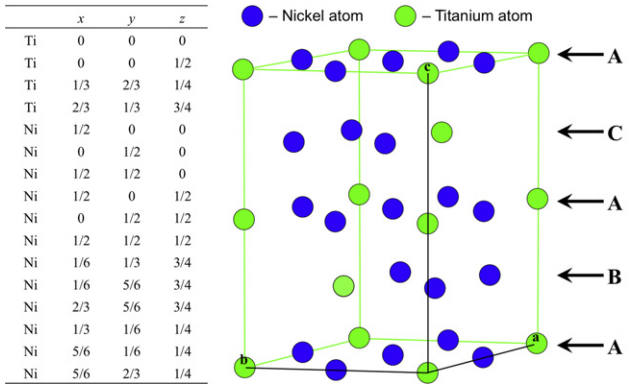

Fig. 7. The unit cell of the η-Ni_3Ti phase and a complete list of the 16 sites of the unit cell.

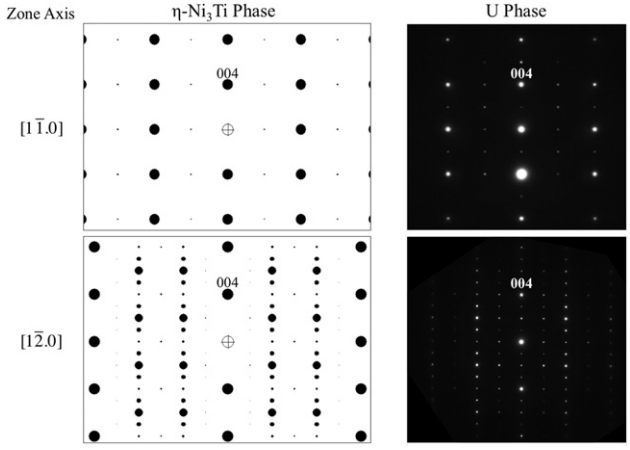

Fig. 8. Comparing simulated diffraction patterns for the η-Ni_3Ti phase and the experimental diffraction patterns obtained at zone axes orientations of [1$\bar{1}$.0] and [1$\bar{2}$.0].

For the η-Ni_3Ti structure, because it is already a close-packed structure, introduction of a third element into the system would likely take place by substitution of certain atomic site(s) in the unit cell; Ta (Nb) atoms should preferably occupy Ti sites as stated earlier. The η-Ni_3Ti unit cell has 16 atomic sites in total, 4 of which are Ti sites and the rest are Ni sites.

We first introduced 1 Ta atom into the unit cell. By kinematic diffraction patterns, it was seen that if only one of the 4 Ti atoms was replaced by a Ta atom, the {001}, {002} and {003} reflections appeared in both [1$\bar{1}$.0] and [1$\bar{2}$.0] zone axes diffraction patterns of the structure, as shown in Fig. 9. The relative intensities of these reflections may vary depending on which site in the unit cell the Ta atom is substituting. In fact, these reflections would also appear if any one of the 16 sites in the unit cell is replaced by a Ta atom. This is because by doing so, the 6_3 symmetry and the *c* glide plane of the original η structure are lost, so that the reflections {00*l*}, when $l=2n+1$, no longer have vanishing structure factors. The reflections {0,0,2*n*}, when *n* is odd, are also present because of the introduction of the term f_{Ta} into the structure factor, and that $f_{Ni} \neq f_{Ti} \neq f_{Ta}$.

This attempt did produce a matching [1$\bar{2}$.0] kinematic ZAD pattern with the correct number of superlattice reflections. However, the [1$\bar{1}$.0] kinematic ZAD pattern did not match the experimental pattern in that it had too many superlattice reflections. This also revealed an incompatibility in the experimental [1$\bar{1}$.0] and [1$\bar{2}$.0] ZAD patterns regarding the superlattice reflections {001}, {002} and {003}. The [1$\bar{2}$.0] experimental pattern always had all the $n/4\vec{g}_{<004>}$ (n=1, 2, 3) reflections whereas the [1$\bar{1}$.0] experimental pattern always only had $1/2\vec{g}_{<004>}$ reflection and never had $n/4\vec{g}_{<004>}$ (n=1, 3) reflections. The presence of the superlattice reflections along the *c*-axis should be the same even when projecting along two different zone-axis directions, at least kinematically. This can only be explained through the dynamic diffraction in the microscope, i.e. double diffraction.

Double diffraction occurs in hexagonal systems with space group: $P6_3/mmc$, no. 194 [15]. The systematic absence of {00*l*} reflections when $l=2n+1$ in the [11.0] ZAD pattern is due of the presence of the 6_3 screw axis and a *c* glide plane. However, {00*l*} ($l=2n+1$) reflections are almost always visible in the experimental diffraction pattern due to double diffraction. In the case of the U phase, the ABaCA stacking makes it a double hexagonal unit cell. Thus, the first fundamental reflection for the U phase is {004} instead of {002} for ABAB hexagonal structure. Based on this analysis, a second attempt of modifying the η phase unit cell aimed to retain the 6_3 symmetry and the *c* glide plane while making {002} reflection visible.

There are two different sites of Ti in the η phase unit cell as shown earlier in Table 2 and Fig. 7, which are Wyckoff 2*d* and 2*a* sites. Each has two equivalents. Two Ta atoms can be substituted into and ordered on either of the two different sites and this gives

Table 3
Bulk composition of the major elements in the U phase in atomic percentage.

Element	Ni	Co	Cr	Ta	Nb	Ti	Al
Average at%	73.20	6.35	1.06	2.54	1.08	11.51	4.27
Standard deviation	1.2729	.7099	.2109	.2764	.3183	.7433	.9145
Max	75.6162	8.6352	1.5213	3.2323	1.6541	13.4357	6.2219
Min	70.7311	5.0281	.7165	1.9333	.0000	10.2696	2.4526

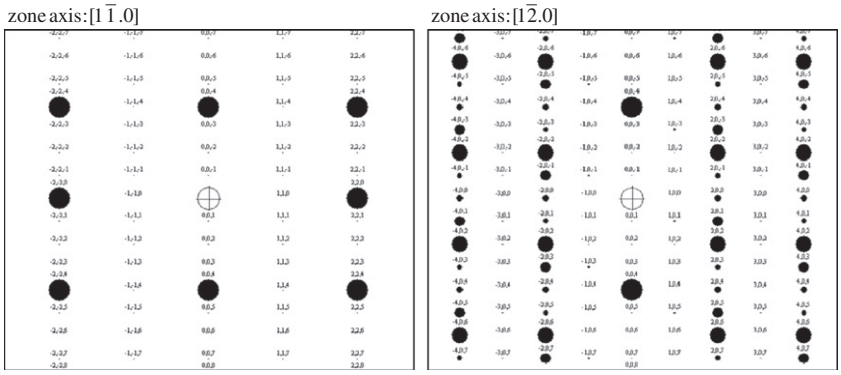

Fig. 9. Simulated [1$\bar{1}$.0] and [1$\bar{2}$.0] zone axis diffraction pattern for substitution of any one of the 16 sites in the unit cell of η phase by a Ta atom (The spots that are labeled by plane indices are the ones allowed for the structure.).

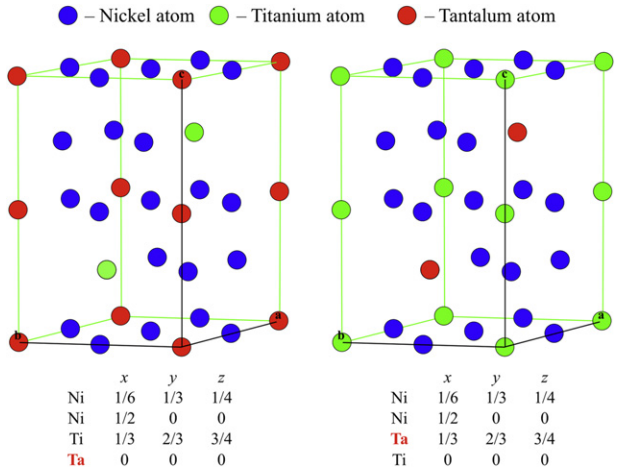

	x	y	z
Ni	1/6	1/3	1/4
Ni	1/2	0	0
Ti	1/3	2/3	3/4
Ta	0	0	0

	x	y	z
Ni	1/6	1/3	1/4
Ni	1/2	0	0
Ta	1/3	2/3	3/4
Ti	0	0	0

Fig. 10. Proposed U phase structures form A (left) and form B (right).

rise to two different derivative structures of ordered η phase, which are shown in Fig. 10. They are called form A and form B, substituting 2*a* and 2*d* sites with Ta atoms, respectively. Such substitution retained the 6_3 symmetry and the *c* glide plane; in fact, the space group remained unchanged as well as the stacking sequence. The reflections {001} and {003} remain extinct because the structure factor contribution from the two equivalents of the 2 sublattices sum to zero. This is shown in Table 4. However, the structure factor for {002} becomes non-zero because the contribution from the Ti on one sublattice can no longer be canceled by the contribution from the other sublattice. Instead, the intensity for {002} becomes 4 $(f_{Ti}-f_{Ta})^2$ or $4(f_{Ta}-f_{Ti})^2$, for form A and form B, respectively, due to the specific ordering of the two Ta atoms introduced.

Furthermore, although Ta atoms preferentially order on one of the Ti sites, there is not enough Ta in the U phase grain to fully occupy one of the Ti sites. According to the STEM–EDS results shown in Fig. 6, the atomic ratio between Ti and Ta is roughly 4.50:1. Therefore, the Ti/Ta ratio on the 2*d* sites is 2.25:1, and this gives the occupancy of Ta to be about .31.

The kinematic ZAD patterns of [1$\bar{1}$.0] and [1$\bar{2}$.0] poles of the proposed structure form B are displayed in Fig. 11. The superlattice reflections in the [1$\bar{1}$.0] pattern match the experimental ones, while the {001} and {003} reflections in the [1$\bar{2}$.0] pattern are missing, as indicated by the open circles and arrows. However, it is easy to see that these missing reflections can be present in the experimental pattern through double diffraction. Because when the 6_3 screw axis and the *c* glide plane in the space group of the structure are directly responsible for the systematic absence of these reflections, double diffraction usually becomes possible. The fact that {001} and {003} reflections vanished in the experimental patterns by tilting the specimen from the [1$\bar{2}$.0] pole to [1$\bar{1}$.0] pole clearly showed these were dynamically diffracted reflections. Therefore, both kinematic ZAD patterns shown in Fig. 11 are in fact consistent with the experimental patterns. Moreover, using the proposed ternary ordered η structures, kinematical ZAD patterns with matching superlattice reflections were also obtained for the rest of the zone-axis directions shown in Figs. 2 and 3.

Since the space group of the two proposed structures, i.e. form A and form B, is the same, the positions of all the reflections in their ZAD patterns would be the same. However, due to the different symmetries of the sublattices on which the Ta atoms order, the relative intensities of the reflections are different for the two. Fig. 12 shows the comparison of the relative intensities of the simulated and experimental reflections of the row [20*n*]* ($n=-2, -1, 0, 1$ and 2) in the [1$\bar{2}$.0] ZAD patterns. The reason for choosing this particular row of reflections for comparison is that these are strong reflections and should be affected less by double diffraction. It is quite clear that the relative intensity of the experimental reflections is similar to that of the form B, which strongly indicates that the Ta atoms tend to order on $\bar{6}$m2 sublattice (Wyckoff 2*d* sites) instead of $\bar{3}$m sublattice (Wyckoff 2*a* sites).

Simulated high-resolution images confirmed that the proposed structure would indeed give the high-resolution images observed in the Titan 80–300 TEM, as shown in Fig. 13a. However, it needs to be pointed out that although the proposed crystal structure form B produces matching electron diffraction patterns to the experimental patterns, its stacking sequence in [00.1] direction, which is ABACA—the same as the η phase, is inconsistent with the intensity difference observed among the "A" and "a" planes in the HR-TEM micrograph (shown in Fig. 5). Since the three planes: (00.0), (00.1/2) and (00.1) in the unit cell are identical in terms of both stacking positions and chemistry, these planes should have appeared with approximately the same intensity in the HR-TEM image.

Through phase-contrast simulation of the tilting effect in the microscope, it was believed that this noticeable intensity difference between the "A" and "a" planes was the result of deviation of the beam direction from the true specimen zone axis orientation in the microscope. It was found that the relative intensities of the "A" and "a" planes can change significantly in a 24 nm thick simulated specimen with a slight deviation as small as 0.87 mrads. Fig. 13b and c show the micrographs simulated for structure form B without and with a deviation of 1.17 mrads, respectively. This is because the "A" planes have neighbor planes in a "CAB" sequence while the "a" planes having neighbor planes

Table 4
Calculated structure factor expressions of the reflections along [004]* direction.

Phase	Reflection	F from $\bar{3}$m sublattice	F from $\bar{6}$m2 sublattice	F^2
η-Ni_3Ti	001	$f_{Ti}(1+e^{\pi i})=0$	$fTi(e^{\pi/2i}+e^{3\pi/2i})=0$	0
	002	$f_{Ti}(1+e^{2\pi i})=2f_{Ti}$	$fTi(e^{\pi i}+e^{3\pi i})=-2fTi$	0
	003	$f_{Ti}(1+e^{3\pi i})=0$	$fTi(e^{3\pi/2i}+e^{9\pi/2i})=0$	0
	004	$f_{Ti}(1+e^{4\pi i})=2f_{Ti}$	$f_{Ti}(e^{2\pi i}+e^{6\pi i})=2f_{Ti}$	$16(fTi+3fNi)^2$
Form A	001	$f_{Ta}(1+e^{\pi i})=0$	$fTi(e^{\pi/2i}+e^{3\pi/2i})=0$	0
	002	$f_{Ta}(1+e^{2\pi i})=2f_{Ta}$	$f_{Ti}(e^{\pi i}+e^{3\pi i})=-2f_{Ti}$	$4(fTa-fTi)^2$
	003	$f_{Ta}(1+e^{3\pi i})=0$	$fTi(e^{3\pi/2i}+e^{9\pi/2i})=0$	0
	004	$f_{Ta}(1+e^{4\pi i})=2f_{Ta}$	$f_{Ti}(e^{2\pi i}+e^{6\pi i})=2f_{Ti}$	$4(fTa+fTi+6fNi)^2$
Form B	001	$f_{Ti}(1+e^{\pi i})=0$	$fTa(e^{\pi/2\cdot i}+e^{3\pi/2\cdot i})=0$	0
	002	$f_{Ti}(1+e^{2\pi i})=2f_{Ti}$	$f_{Ta}(e^{\pi i}+e^{3\pi i})=-2f_{Ta}$	$4(fTi-fTa)^2$
	003	$f_{Ti}(1+e^{3\pi i})=0$	$fTa(e^{3\pi/2\cdot i}+e^{9\pi/2i})=0$	0
	004	$f_{Ti}(1+e^{4\pi i})=2f_{Ti}$	$f_{Ti}(e^{2\pi i}+e^{6\pi i})=2f_{Ti}$	$4(f_{Ta}+f_{Ti}+6f_{Ni})^2$

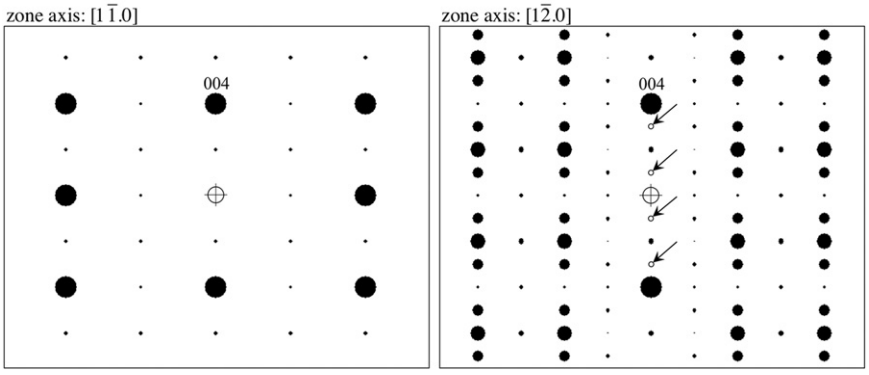

Fig. 11. Simulated [1$\bar{1}$.0] and [1$\bar{2}$.0] zone axis diffraction pattern for the proposed structure form B.

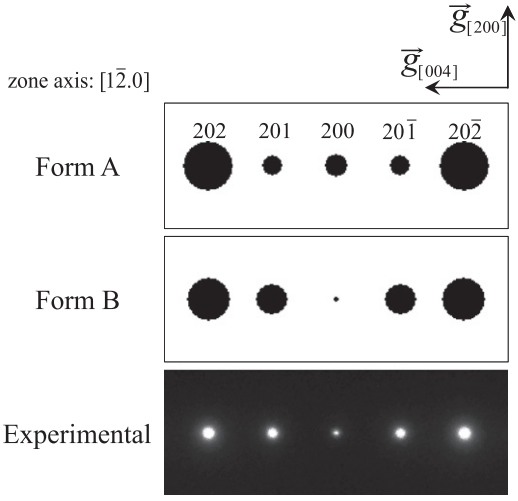

Fig. 12. Comparison of the relative intensities of the simulated and experimental reflections of the row [20n]* in the [1$\bar{2}$.0] ZAD patterns.

in a "BaC" sequence. In other words, the angles of the inter-planar bonds are oriented differently. It turned out that the "BaC" stacking sequence was affected more by the deviation from the true zone axis orientation than the "CAB" sequence. For this reason, we refer to the stacking sequence of the proposed U phase structure as A<u>B</u>A′<u>C</u>A, so as to distinguish the (00.0), (00.1/2) and (00.1) planes. The underline for B and C planes shows that they have different chemistry than A planes.

It can therefore be concluded that the Ta atoms preferably ordered on the Wyckoff 2*d* sites. A ternary-ordered η phase (i.e. Ni_6AlNb) has also been reported in the newly developed Allvac 718Plus Ni-based superalloy, in which the authors concluded that the Nb ordered on the Wyckoff 2*a* sites while Al and Ti randomly occupied the 2*d* sites [14]. Tantalum and Nb belong to the same column in the periodic table and their radii are similar. The difference in the ordering sites shown in this study may be attributed to the atomic interaction between the Ta atoms and their nearest and second nearest neighbors or possibly third nearest neighbors.

Future investigation of this derivative phase of the ordered η-Ni_3Ti is needed with respect to the effects of the decomposition of the strengthening γ' precipitates and subsequent phase transformation on the mechanical integrity of the alloy. Experimental measurements of the mechanical properties of the U phase would be desirable, such as yield strength, hardness, etc. However, the small size of these precipitates would pose experimental challenges on such attempts. Synthesizing this intermetallic phase from model alloys of simple ternary systems can be therefore considered. Moreover, the mechanical response of the entire sub-surface region compromised by oxidation under the turbine service environment should be examined for potential mechanical failures.

5. Conclusion

The high-temperature-oxidation of Inconel 939 Ni-based superalloy exposed to oxy-fuel combustion environment for up to 1000 h induced a phase transformation in the sub-surface region, and a two-phase region formed at the expense of strengthening γ' precipitates. The oxidation microstructure typically consisted of an external scale, an internal oxidation zone and a twinning zone, i.e. Ni-matrix and an unknown phase abbreviated as the U phase. Through electron microscopy studies, the

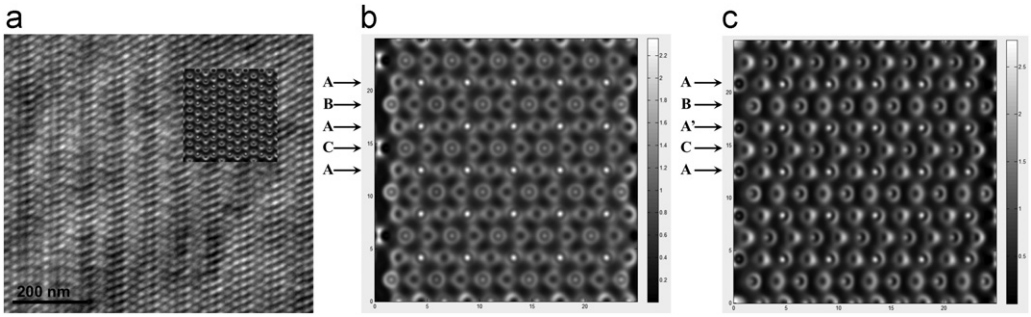

Fig. 13. (a) Simulated high-resolution image embedded in the experimental micrograph. Simulated image of a 24 nm thick specimen with (b) no tilt and (c) with a tilt of 1.17 mrads.

crystal structure of the U phase can be modeled as a ternary derivative of the ordered η-Ni_3Ti phase ($D0_{24}$) structure with the following parameters:

- The ordering occurred in a ternary system of Ni–Ti–Ta, in which the Ta ordered on the Wyckoff 2*d* sites with occupancy of .31.
- The lattice parameters are: a=.5092 nm and c=.8336 nm; $\alpha=90^\circ$, $\beta=90^\circ$ and $\gamma=120^\circ$.
- The space group is $P6_3/m\ 2/m\ 2/c$ (no. 194) and the Pearson symbol is *hP*16.
- The stacking sequence is $A\underline{B}A'\underline{C}A$.
- The orientation relationship between the U phase and the Ni-matrix (γ solid solution) is

$$(11\bar{1})_\gamma \| (00.1)_\eta$$

$$[1\bar{1}0]_\gamma \| [2\bar{1}.0]_\eta$$

Further studies on the mechanical properties of the U phase and its surrounding regions can add to the knowledge on the effects of the decomposition of the strengthening γ' precipitates.

Acknowledgment

This technical effort was performed in support of the National Energy Technology Laboratory's ongoing research in advanced combustion technology under the RES contract DE-FE0004000.

References

[1] R.E. Anderson, F. Viteri, R. Hollis, M. Hebbar, J. Downs, D. Davies, M. Harris, ASME Turbo Expo 2009: Power for Land, Sea and Air, ASME, Orlando, FL, 2009.
[2] W. Sanz, H. Jericha, F. Luckel, E. Göttlich, F. Heitmeir, ASME Turbo Expo 2005: Power for Land, Sea and Air, ASME, Reno-Tahoe, Nevada, USA, 2005.
[3] Indranil Roy, Ph.D. Thesis, Precipitate Growth Features in the Duplex Size Gamma Prime Distribution in the Superalloy In738LC, Louisiana State University, 2003.
[4] G.R. Holcomb, P. Wang, in: D. Gandy, J. Shingledecker, R. Viswanathan (Eds.), Proceedings of the 6th International Conference on Advances in Materials Technology for Fossil Power Plants, EPRI Report no. 1022300, ASM International, Materials Park, OH, 2011, pp. 312–324.
[5] T.B. Gibbons, R. Stickler, in: R. Brunetaud, et al., (Eds.), High Temperature Alloys for Gas Turbines, D. Reidel Publishing Co., Dordrecht, 1979, p. 369.
[6] Z. Mišković, M. Jovanović, M. Gligić, B. Lukić, Vacuum 43 (1992) 709–711.
[7] J. Zhu, G.R. Holcomb, P.D. Jablonski, A. Wise, J. Li, D.E. Laughlin, S. Sridhar, Mater. Sci. Eng. A 550 (2012) 243–253.
[8] Thermo-Calc, Version S, Thermo-Calc Software AB, Stockholm, Sweden, 2008.
[9] C.T. Koch, Ph.D. Thesis, Determination of Core Structure Periodicity and Point Defect Density along Dislocations, Arizona State University, 2002.
[10] D.J. Young, High Temperature Oxidation and Corrosion of Metals, Elsevier Ltd., Jordan Hill, UK, 2008.
[11] F. Laves, H.J. Wallbaum, Ziet. Krystall. 101 (1939) 78–93.
[12] Pearson's Crystal Data. Data Sheet of: 1617076. Copyright© 2007 ASM International® and Material Phases Data System.
[13] G. Sauthoff, Intermetallics, Weinheim VCH, New York, 1995.
[14] E.J. Pickering, H. Mathur, A. Bhowmik, O.M.D.M. Messe, J.S. Barnard, M.C. Hardy, R. Krakow, K. Loehnert, H.J. Stone, C.M.F. Rae, Acta Mater. 60 (2012) 2757–2769.
[15] M. De Graef, Introduction to Conventional Transmission Electron Microscopy, Cambridge University Press, Cambridge, UK, 2003.